Technology Update

Benefit of Cone-Beam CT Angiography in Visualizing Aneurysm Shape and Identification of Exact Rupture Site

Alexandra Lauric, PhD, Robert S. Heller, MD, Sarah Schimansky, BS, Adel M. Malek, MD, PhD

From the Cerebrovascular and Endovascular Division, Department of Neurosurgery, Tufts Medical Center and Tufts University School of Medicine, Boston, MA.

ABSTRACT

While high-resolution cone-beam computational tomographic (CBCT) angiography has gained use in intracranial vascular imaging, digital subtraction angiography (DSA) and 3-dimensional-rotational angiography (3D-RA) remain the preferred acquisition modalities for intracranial aneurysm imaging. This case report highlights the utility of the greater spatial resolution afforded by CBCT for cerebral aneurysm imaging. A 54-year-old man presenting with subarachnoid hemorrhage was confirmed to harbor a ruptured anterior communicating artery aneurysm by conventional angiography. Due to varying contrast opacification captured by different acquisition methods, dramatic aneurysm shape difference was observed between 2- and 3-dimensional-angiographic and CBCT models. The greater resolution of CBCT revealed in an unequivocal fashion the exact site of rupture on the aneurysm dome, visualized as a discrete irregular and elongated bleb that was not seen on either 3D-RA or DSA. High-resolution CBCT visualized the shape of the target aneurysm in greater detail than the more conventional 2D-DSA and 3D-RA, enabling more precise computational fluid dynamics (CFD) simulations. Given that aneurysms most likely change shape either prior to rupture or upon rupture, future studies evaluating fluid dynamics using computer reconstructions should be cognizant of the differences in resolution provided by various imaging modalities.

Keywords: Intracranial aneurysm, rupture site, subarachnoid hemorrhage, computational fluid dynamics, wall shear stress, cone-beam computed tomography.

Acceptance: Received July 10, 2013, and in revised form January 23, 2014. Accepted for publication January 27, 2014.

Correspondence: Address correspondence to Adel M. Malek, MD, PhD, Department of Neurosurgery, Tufts Medical Center, 800 Washington Street, Boston, MA 02111. E-mail: amalek@tuftsmedicalcenter.org.

Disclosures: This work was supported by NIH-R21HL102685. AMM has received unrestricted research support from Microvention Inc., Stryker Neurovascular, Codman Neurovascular, Siemens Inc., Ansys Inc., and CD-Adapco for unrelated work.

J Neuroimaging 2015;25:56-61.
DOI: 10.1111/jon.12120

Background and Importance

Aneurysmal subarachnoid hemorrhage is often a devastating event that, despite advancements in patient management, still carries a mortality rate of 40-50% and a morbidity rate of 10-20%. While digital subtraction angiography (DSA) is generally used as the gold standard in intracranial aneurysms imaging, 3-dimensional-rotational angiography (3D-RA) is considered a major step forward in the detection and evaluation of intracranial aneurysms.[1] Increasingly, high-resolution cone-beam computational tomographic angiography (CBCT-A) has gained use in vascular intracranial imaging, particularly for its ability to detect hemorrhage, its use in follow-up of stent therapy, and characterization of atherosclerotic lesions.[2]

The mechanism of aneurysm rupture is poorly understood, and research findings are often contradictory. It has been suggested that, in the absence of underlying disease, aneurysm formation and evolution is a mechanically mediated event.[3] Clinical and experimental studies strongly suggest that hemodynamic factors play a role in aneurysm formation, growth, and eventual rupture, although the exact contribution is not completely understood.[4] Most often, clinicians rely on morphological analysis of the size and shape of the aneurysms to explain rupture or to predict the rupture likelihood of unruptured aneurysms. However, retrospective morphological analysis relies on the assumption that rupture does not affect the size and shape of aneurysms,[5] a hypothesis that has yet to be conclusively proven.

Herein, we report the case of a ruptured anterior communicating artery aneurysm, for which high-resolution CBCT-A revealed the exact site of rupture, as an elongated plume of contained contrast emanating from the surface of a daughter component. This level of detail was not evident on 3D-RA, DSA, or multidetector computed tomographic angiography (CTA). The ability to pinpoint the rupture site was afforded by the greater sensitivity and surface detail provided by CBCT-A, which allowed computational fluid dynamics (CFD) analysis of the rupture region.

 Copyright © 2014 by the American Society of Neuroimaging

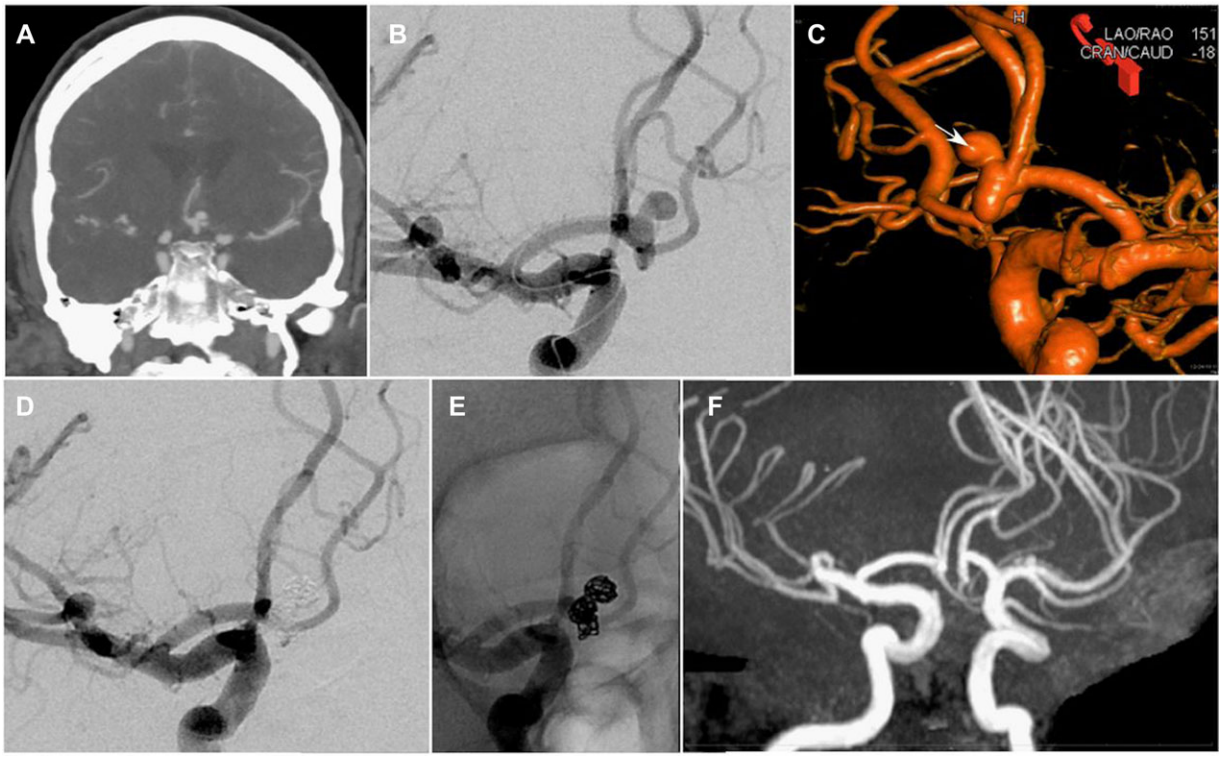


Fig 1. Computed tomographic angiography (CTA) of patient with subarachnoid hemorrhage revealing a ruptured anterior communicating artery aneurysm (A). Digitally subtracted angiography (DSA) of right internal carotid artery injection (B) shows a smooth contoured bilobed aneurysm. 3D-RA volumetric reconstruction from a posterior projection reveals a possible smooth focal bleb (C, arrow). Aneurysm underwent successful coil embolization (D, DSA; E, fluorogram), with no residual on 3-Tesla magnetic resonance angiography (MRA) follow-up at 2 years (F).

Clinical Presentation

History and Presentation

A 54-year-old man suffered a syncopal episode lasting 5 minutes, followed by headache and nausea. The patient underwent computed tomography angiogram (CTA) showing subarachnoid hemorrhage and a ruptured anterior communicating artery aneurysm (Fig 1). The patient was transferred to our facility for further evaluation and treatment. Within 12 hours of ictus, he underwent cerebral angiography on a calibrated flat-panel biplanar DSA system (Artis, Siemens, Malvern, PA, USA). Conventional DSA was performed of the right internal carotid artery (Fig 1), which was followed by 3D-RA (5 seconds acquisition, 3 cc/second contrast injection with 1 second preinject) and CBCT-A (20 seconds acquisition, 1 cc/second contrast injection with 2 seconds preinject) immediately after.

Acquisitions were reconstructed using a Leonardo software package (Siemens) to yield 3-dimensional volumetric data sets including the aneurysm and parent vessels, which were segmented in Amira, (version 5.4, Visage Imaging, San Diego, CA, USA). Parameters for the 20-second CBCT-A acquisition were kVP = 70 kV, mas = 1.2 μGy/pulse, and focal point = .6 mm. No mask run was performed prior to acquisition; resolution of the reconstruction was .095 mm.[3] The radiation dose was 212 μGy with injection of 22 cc of contrast.

All imaging sets revealed a bilobed ruptured anterior communicating artery aneurysm with an irregular shape pointing anteriorly and superiorly (Fig 2). Three-dimensional RA (Figs 2C and D) provided significantly better detail than the corresponding CTA (Figs 2A and B). In contrast to 3D-RA (Figs 2C and D), CBCT-A (Figs 2E and F) revealed a well-defined area of contrast medium linking the rupture site on the dome to the adjacent tamponading hematoma in the subarachnoid space. This rupture site is situated at the most distal point of the aneurysm dome on the daughter aneurysm pointing superiorly and laterally. There were no changes in the patient's vital signs or intracranial pressure during or after the CBCT-A acquisition, which was performed at the very low rate of 1 cc/second injection. The aneurysm was successfully coiled (Fig 1) and the patient discharged with a modified Rankin score of 0 on day 14; he is asymptomatic at the 2-year follow-up without residual on 3-Tesla magnetic resonance angiography (MRA). Follow-up imaging has shown no residual aneurysm filling at up to 2 years postop (Fig 1F).

Hemodynamics Simulation and Analysis

A 3-dimensional model derived from the 3D-RA segmented data and describing the aneurysm as well as its adjacent parent vessels was available for analysis. High-resolution tetrahedral meshes with prismatic boundary layer enrichment were

15526569, 2015, 1, Downloaded from https://onlinelibrary.wiley.com/doi/10.1111/jon.12120 by Tufts University, Wiley Online Library on [15/11/2026]. See the Terms and Conditions (https://onlinelibrary.wiley.com/terms-and-conditions) on Wiley Online Library for rules of use; OA articles are governed by the applicable Creative Commons License

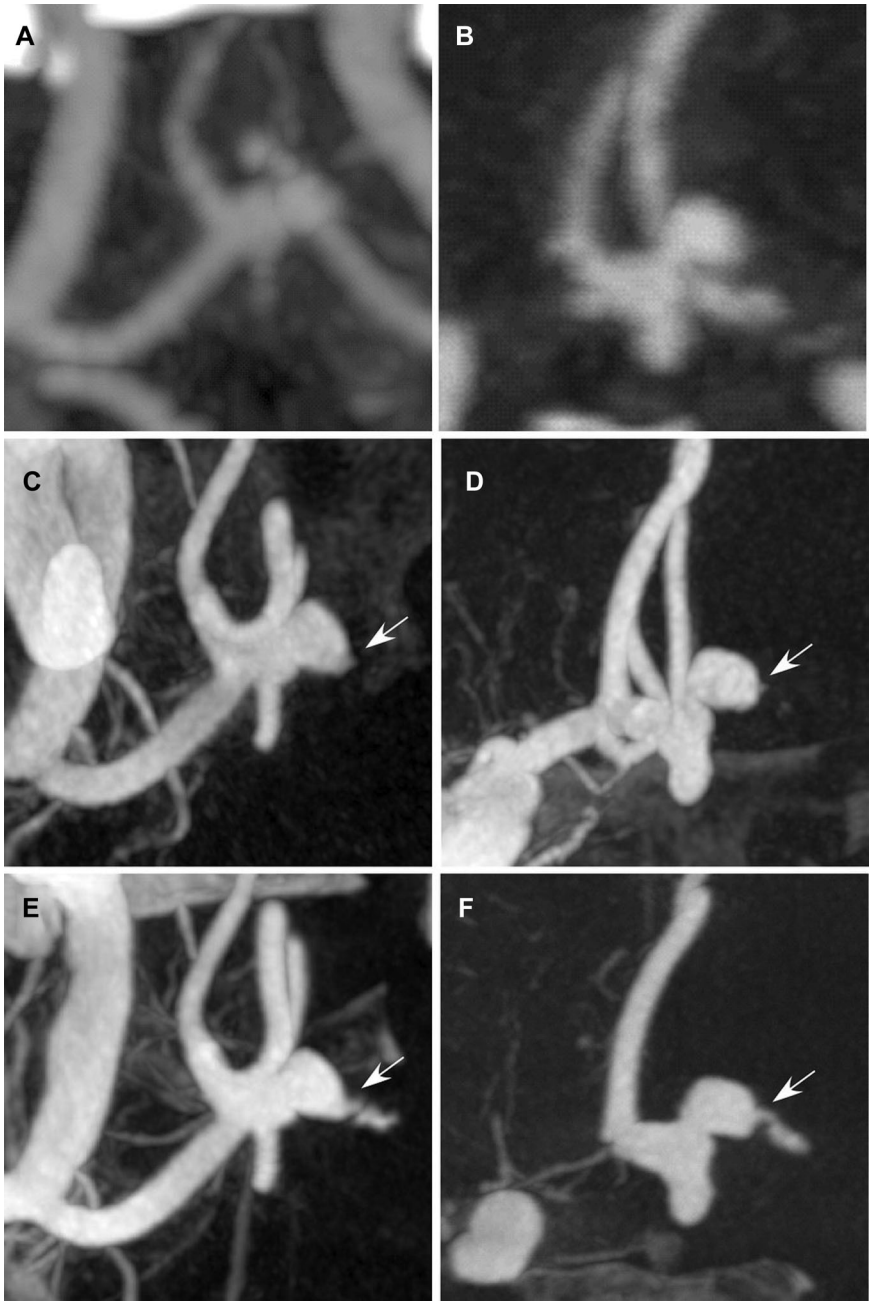


Fig 2. Angiographic imaging of a right bilobed ruptured anterior communicating artery aneurysm. Multiplanar reconstruction using maximum intensity projection of the in-axial (A, C, E) and coronal (B, D, F) orientation. Top (A, B) shows multidetector CTA for comparison. Three-dimensional rotational angiogram (3D-RA) (C, D) reveals a minuscule protuberance (arrow). Cone-beam computed tomographic angiogram CBCT-A (E, F) clearly shows the contrast medium communicating from the point of rupture on the dome to the tamponading hematoma in the subarachnoid space.

generated with Harpoon version 4.4 (Sharc Ltd., Manchester, UK) at a count of 1,245,000 cells. Fluent version 13.0 (Ansys, Lebanon, NH, USA) was used to perform mesh conversion to polyhedral domain followed by finite-volume solution in the laminar double-precision unsteady regime, assuming rigid non-slip wall conditions, blood viscosity of .04 P, and density of 1000 kg/m.[3] The simulations were run for two cardiac cycles, before being reported for the third cycle. The pulsatile flow boundary conditions were based on the flow rate waveform used by Steinman et al,[6] which was scaled such that the mean wall shear stress (WSS) value in the inflow parent vessel (diameter 2.3 mm) was approximately 1.5 Pa. This resulted in a mean flow rate of .5 mL/second, which was used as an inlet boundary condition, with zero pressure boundary condition at the outlets. The average Reynold's number proximal to the aneurysm neck was 67.71 and the Womersley number was 1.44.

15526569, 2015, 1, Downloaded from https://onlinelibrary.wiley.com/doi/10.1111/jon.12120 by Tufts University, Wiley Online Library on [15/11/2026]. See the Terms and Conditions (https://onlinelibrary.wiley.com/terms-and-conditions) on Wiley Online Library for rules of use; OA articles are governed by the applicable Creative Commons License

Table 1. Maximum and Mean Values of WSS, WSSG, and OSI, were Computed over the Whole Cardiac Cycle, on the Four Regions Studied: the Rupture Site, the Hosting Daughter Aneurysm, the Whole Aneurysm, and Adjacent Vessels; Mean and Standard Deviation Are Reported

	Rupture Site	Daughter Aneurysm	Whole Aneurysm	Adjacent Vessels
Max WSS (Pa)	.03	1.64	8.97	18.41
Mean WSS (Pa)	.003 ± .005	.03 ± .06	.25 ± .54	1.74 ± 1.42
Max WSSG (Pa/m)	69.6	11,766.8	60,678.3	45,415.2
Mean WSSG (Pa/m)	5.81 ± 10.6	49.46 ± 220	355.86 ± 1,069	1,784.9 ± 2,291
Max OSI	.10	.47	.47	.31
Mean OSI	.08 ± .01	.03 ± .05	.02 ± .04	.005 ± .02

WSS = wall shear stress; WSSG = spatial WSS gradient; OSI = oscillatory shear index.

Postprocessing was performed using Ensight Version 9 (CEI, Apex, NC, USA). WSS, the spatial WSS gradient (WSSG),[7] and the oscillatory shear index (OSI)[7] were evaluated on four different regions: (1) the base of the small bleb representing the rupture site (area 1.35 mm^2), (2) the superiorly directed spherical daughter aneurysm hosting the rupture site (area 51.75 mm^2), (3) the entire aneurysm (area 105.76 mm^2), and (4) adjacent vessels area, containing the neck of the aneurysm and approximately one diameter along each of the vessels touching the neck of the aneurysm (area 55.34 mm^2). Maximum and average values were recorded for the three parameters (WSS, WSSG, and OSI). In the case of time-dependent parameters (WSS and WSSG), the time-averaged mean was computed over the whole cardiac cycle. Maximum and mean OSI values were evaluated spatially over the four regions.

As shown in Table 1, the site of rupture corresponds to the lowest WSS and WSSG magnitude values, both in terms of maximal values as well as temporal means. Specifically, WSS values at the site of rupture (max value .03 Pa) were much smaller compared to WSS values on the rest of the daughter aneurysm (max value 1.64 Pa), which in turn are lower than WSS values on the whole aneurysm (max value 8.97 Pa). Regardless of the aneurysm region, both maximum and mean WSS on the surface of the aneurysm were lower than those on the adjacent vessels. Similarly, WSSG values on the surface of the aneurysm (max value 69.59 Pa/m) were much lower compared to WSSG values on the rest of the daughter aneurysm (max value 11,766.8 Pa/m), which in turn are lower than WSSG values on the whole aneurysm (max value 60,678.3 Pa/m). Regardless of the aneurysm region, WSSG values on the surface of the aneurysm were lower than those on the adjacent vessels.

OSI values on the aneurysm surface were clearly higher compared to values on the adjacent vessels (mean OSI .02 vs. .005). Similarly, OSI at the site of rupture was elevated but not maximal at that spot and appeared lower than nearby regions on both the superiorly directed daughter portion or of the whole aneurysm (Table 1). Figures 3A–C show WSS, WSSG, and OSI distributions at end-diastole. Although WSS values at the rupture site fluctuated over the cardiac cycle, they were consistently lower than WSS on the hosting daughter aneurysm, as well as WSS on the surface of the entire aneurysm.

Discussion

While DSA is still considered the gold standard in intracranial aneurysms imaging, research suggests that 3D-RA has many advantages over DSA and should be recommended as the optimal image strategy in patients with suggestion of intracranial aneurysms.[1] Where available, high-resolution CBCT has proven valuable in its ability to characterize vascular pathology in greater detail than conventional angiography.[2,8] The case reported herein is a demonstration of the exact aneurysm rupture site being visualized by CBCT-A imaging in unequivocal fashion.

Although CTA, DSA, 3D-RA, and CBCT-A data were available during the same procedure, only CBCT-A images visualized the area of rupture. Beyond the higher sensitivity of CBCT, it is possible that the contribution of its longer acquisition time (20 seconds for CBCT vs. 5 seconds for 3D-RA) could have allowed contrast from the aneurysm dome to diffuse into the tamponading hematoma adjacent to the rupture site. In the acute rupture setting, partial thrombosis of the aneurysm could potentially prohibit visualization of the entire aneurysm. Although the images provided by CBCT-A may show diffusion along a path between clot of different levels of organization, the ability to track the contrast back to the aneurysm dome and the sharp bleb seen on 3D-RA both argue in favor of its being the exact rupture site. This study illustrates that CBCT-A may enable more accurate visualization of the entire aneurysm than 3D-RA alone, especially with regards to its point of decompression into adjacent brain, arachnoid, or pseudoaneurysm versus partial thrombosis. The ability to pinpoint the rupture site allowed for hemodynamic analysis of that region. It was previously shown that low WSS and high OSI, by causing degenerative changes in the aneurysm wall, may facilitate the growth of the aneurysm wall, which could potentially lead to rupture.[9] Our analysis showed the rupture site to be characterized by very low WSS compared to WSS values on the rest of the aneurysm dome. In fact, the maximum WSS of the rupture site was 50 times lower than the maximum WSS of the host daughter aneurysm and 300 times lower than the maximum WSS value average over the whole aneurysm. Similarly, WSSG of the rupture site was much smaller as compared to the rest of the aneurysm. Maximum WSSG of the rupture site was 170 times smaller than maximum WSSG of the daughter aneurysm, and 879 times smaller than the maximum WSSG of the whole aneurysm.

These results suggest that flow stasis and associated low WSS are spatially linked with rupture, rather than high WSS as suggested by others.[10,11] Similar to previous research, we found that OSI values on the surface of the aneurysm were higher than OSI of adjacent vessels; however OSI did not seem to

15526569, 2015, 1, Downloaded from https://onlinelibrary.wiley.com/doi/10.1111/jon.12120 by Tufts University, Wiley Online Library on [15/11/2026]. See the Terms and Conditions (https://onlinelibrary.wiley.com/terms-and-conditions) on Wiley Online Library for rules of use; OA articles are governed by the applicable Creative Commons License

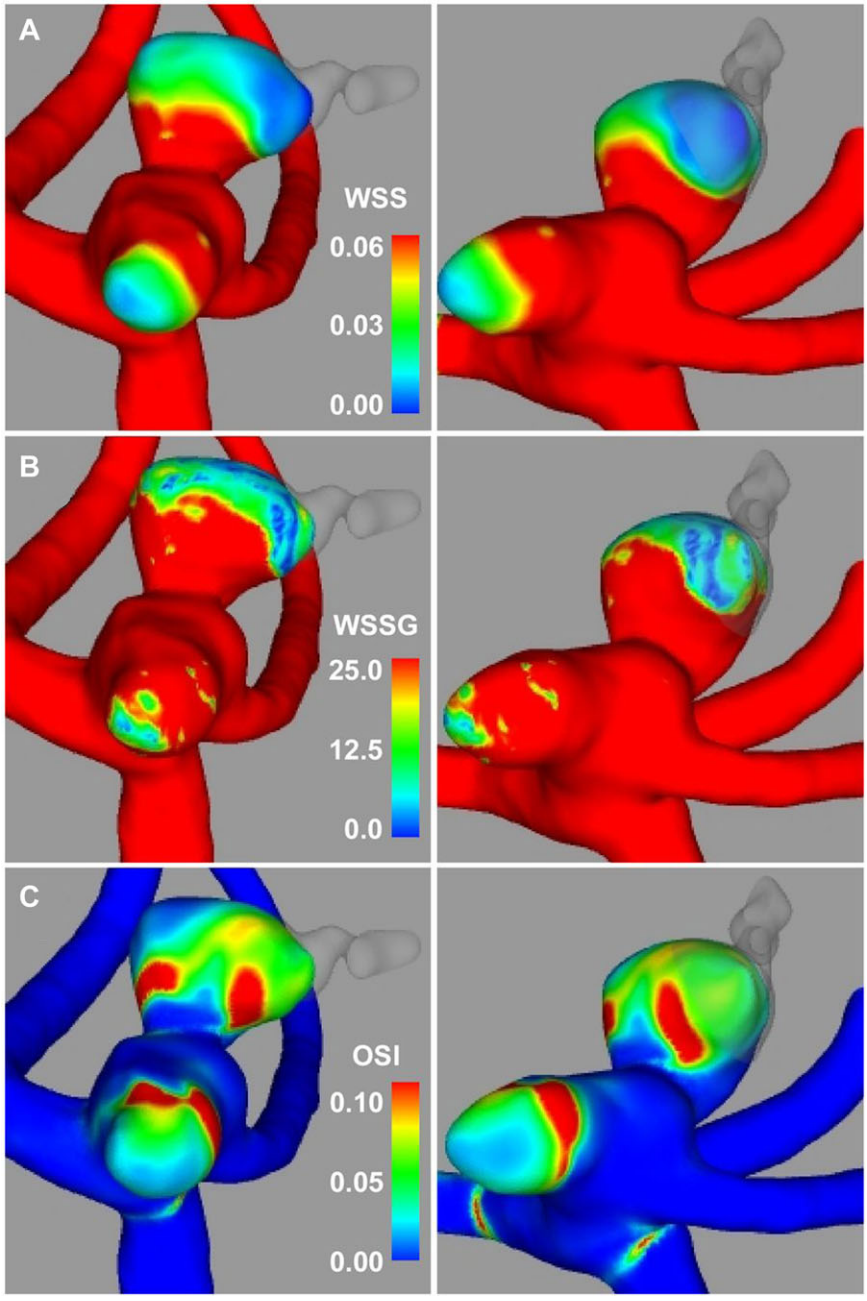


Fig 3. End-diastole distribution of (A) WSS, (B) WSSG, and (C) OSI. In each case the aneurysm is shown from two viewing positions. Hemodynamic simulation was performed on 3D-RA data. CBCT-A model, showing the rupture site and contrast extravasation plume, was superimposed on the 3D-RA model for indication of the rupture site. The rupture site is characterized by low WSS, low WSSG, and higher OSI.

discriminate between the rupture site and the rest of the aneurysm. Although a single case, the report further enforces the link between low WSS and wall degeneration leading to rupture.

This report suggests that the diffusion of the contrast media into the rupture site, depending on how much of this process is captured during acquisition, may affect the resulting aneurysm models and all subsequent morphological analysis. Retrospective morphological analysis of aneurysmal lesions are based on the assumption that aneurysm do not change shape and size after rupture. While previous research[5,10] argued that indeed this assumption holds true, the clinicians should be aware of this potential diffusion artifact, which may not be always recognized as contrast opacification.

The serendipitous finding of a likely qualitatively weak spot in the aneursysm wall was the major impetus for the CFD analysis contained herein. By determining the WSS relative value at that location, the aim of this analysis was to provide additional objective data obtained using the emerging technique of CBCT-A. However, as a single case, this analysis is not intended to be

15526569, 2015, 1, Downloaded from https://onlinelibrary.wiley.com/doi/10.1111/jon.12120 by Tufts University, Wiley Online Library on [15/11/2026]. See the Terms and Conditions (https://onlinelibrary.wiley.com/terms-and-conditions) on Wiley Online Library for rules of use; OA articles are governed by the applicable Creative Commons License

definitive as the current study is limited by the likely effects of approximated boundary conditions and the relative influence of the viscosity model employed. Additionally, the CFD simulations did not consider flow contribution from the left A1 artery, which may have affected the observed results.[11]

As highlighted by this report, CBCT may provide greater spatial resolution for pathology of the cerebral vasculature than other commonly used imaging modalities such as DSA and 3D-RA. With the high level of detail provided by CBCT, the findings on CFD could be more precisely correlated with the exact site of rupture on the aneurysm. Given that aneurysms may change shape either prior to rupture or upon rupture, the ability of CBCT to depict aneurysm shape with greater specificity endorses its utility in complex simulations. Accurate analysis of CFD, which appears to be facilitated by CBCT, will aid in identifying those aneurysms more susceptible to rupture.

Conclusion

The case presented herein illustrates the utility of CBCT angiography in identifying additional details of intracranial lesions that are not easily identifiable on other currently available angiographic modalities. This facilitated a more accurate hemodynamic simulation, which provided unequivocal support to identification and correspondence of the exact rupture site with the area of lowest WSS and elevated OSI. Morphological analysis of aneurysmal lesions is based on the assumption that aneurysms do not change shape and size at rupture. This case reports suggest that CBCT enables high-resolution analysis of aneurysm shape, which may be important in identifying alterations in aneurysm shape associated with rupture.

References

1. van Rooij WJ, Sprengers ME, de Gast AN, et al. 3D rotational angiography: the new gold standard in the detection of additional intracranial aneurysms. *Am J Neuroradiol* 2008;29(5):976-979.
2. Heller RS, Malek AM. Successful detection of embologenic ulceration in a symptomatic non-hemodynamic intracranial stenosis using C-arm cone beam CT. *J NeuroIntervention Surg* 2013;5(2): doi:10.1136\neurintsurg-2011-010206. Epub 2012 Jan 21.
3. Foutrakis GN, Yonas H, Sclabassi RJ. Saccular aneurysm formation in curved and bifurcating arteries. *Am J Neuroradiol* 1999;20(7):1309-1317.
4. Sforza DM, Putman CM, Cebral JR. Hemodynamics of cerebral aneurysms. *Ann Rev Fluid Mech* 2009;41(1):91-107.
5. Rahman M, Ogilvy CS, Zipfel GJ, et al. Unruptured cerebral aneurysms do not shrink when they rupture: multicenter collaborative aneurysm study group. *Neurosurgery* 2011;68(1):155-160; discussion 160-161.
6. Steinman DA, Hoi Y, Fahy P, et al. Variability of computational fluid dynamics solutions for pressure and flow in a giant aneurysm: the ASME 2012 Summer Bioengineering Conference CFD Challenge. *J Biomech Eng* 2013;135(2):021016 (13 pp).
7. Buchanan JR, Kleinstreuer C, Truskey GA, et al. Relation between non-uniform hemodynamics and sites of altered permeability and lesion growth at the rabbit aorto-celiac junction. *Atherosclerosis* 1999;143(1):27-40.
8. Patel NV, Gounis MJ, Wakhloo AK, et al. Contrast-enhanced angiographic cone-beam CT of cerebrovascular stents: experimental optimization and clinical application. *Am J Neuroradiol* 2011;32(1):137-144.
9. Shojima M, Oshima M, Takagi K, et al. Magnitude and role of wall shear stress on cerebral aneurysm. *Stroke* 2004;35(11):2500-2505.
10. Asari S, Ohmoto T. Natural history and risk factors of unruptured cerebral aneurysms. *Clin Neurol Neurosurg* 1993;95(3):205-214.
11. Jou LD, Lee DH, Mahwad ME. Cross flow at the anterior communicating artery and its implication in cerebral aneurysm formation. *J Biomech* 2010;43(11):2189-2195.

15526569, 2015, 1, Downloaded from https://onlinelibrary.wiley.com/doi/10.1111/jon.12120 by Tufts University, Wiley Online Library on [15/11/2026]. See the Terms and Conditions (https://onlinelibrary.wiley.com/terms-and-conditions) on Wiley Online Library for rules of use; OA articles are governed by the applicable Creative Commons License